

PERMEABILITY PREDICTION USING A MULTIGRID METHOD

R. Loendersloot^{1,3}, W.J.B. Grouve², R. Akkerman², S. van den Berg²

¹ *Reden – Research Development Nederland, Twekkelerweg 263, 7553 LZ Hengelo, The Netherlands: r.loendersloot@reden.nl*

² *Chair of Production Technology, Faculty of Engineering Technology, University of Twente, P.O. Box 217, 7500 AE Enschede, The Netherlands: r.akkerman@utwente.nl*

³ *Corresponding Author's Email: r.loendersloot@reden.nl*

SUMMARY: A finite difference based Stokes solver is developed to predict the mesoscopic permeability of textile reinforcements. In general, a high grid resolution is employed (either globally or locally) to capture the geometrical details of the reinforcement. Local grid refinements often result in poor aspect ratios of the elements, resulting in inaccurate results, whereas the computational cost of complete fine grid models is extremely high, if not too high for practical use. A Multigrid method is implemented to combine computational efficiency with accuracy. The fine grid levels allow a sufficiently accurate description of the internal geometry of the fabric, whereas the coarse grid levels ensure a sufficiently fast convergence for practical use of the solver. The Multigrid Stokes solver is validated on experimental and numerical results found in literature. It can be concluded that the performance of the solver is excellent, for both high and low fibre contents. The solver is currently being used to investigate the transverse permeability of fabric used for CETEX[®] fabric reinforced thermoplastic plates.

KEYWORDS: multigrid, permeability, internal geometry

INTRODUCTION

A wide variety of flow solvers to solve the resin flow through a dry fibrous preform is presented in the past. They are either based on analytical solutions, or employing (semi-)commercial codes. However, most of them are limited to a relatively basic representation of the internal geometry of the fabric, whereas simultaneously a development is going on to describe the internal geometry of a fabric in more detail [1, 2]. The latter is desirable, as higher fibre contents are applied, which require more detail in the models predicting the flow through dense fibre beds. As a consequence, the models grow in the sense of complexity, but also in terms of required computational effort. Applicability outside the academic world becomes virtually impossible. Simplified geometries

are often employed to obtain reasonable calculation times, accepting the reduced accuracy of the models.

The Multigrid solver presented here, attempts to combine computational performance with high level detail in the description of the internal geometry of the fabric. This article first briefly describes the internal geometry of a fabric. An explanation of the Multigrid solution methodology follows and the article is finalized with the first results of the solver, compared to solution found in the literature.

GEOMETRICAL DESCRIPTION OF FABRICS

The reinforcement is modeled here at the meso-level scale that is at the typical length scale of the fibre bundles ($\sim 10\text{-}1\text{ mm}$). This implies that the internal geometry of the bundle is neglected. The latest developments on a methodology to account for microscopic flows are presented by Groupe and Akkerman [3]. The meso-level solver is constructed such that functions to account for the micro-level flow can be implemented straightforwardly, as it is the final goal here to build a solver for the entire fluid domain. The three length scales (macro level for the fabric length scale) are shown in Fig. 1.

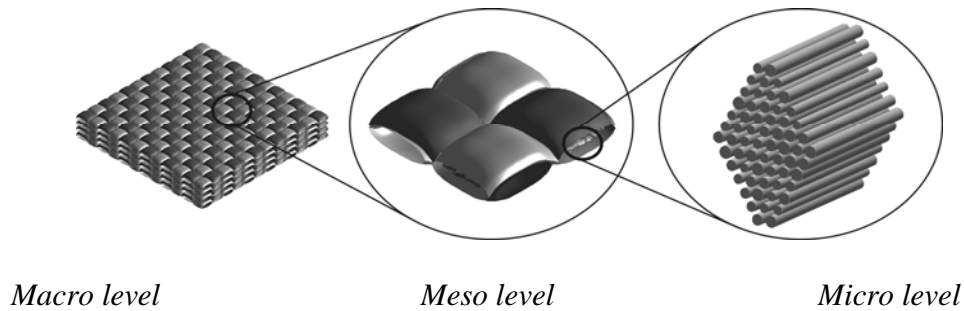


Fig. 1 The three typical length scales as generally employed in composite modeling.

The fibre bundles in reinforcement are often represented by idealized shapes, such as sinusoidal or elliptical shapes for example. The derivation of the geometrical functions is not of interest here, since the fluid flow solver is developed independently, allowing the implementation of any geometry descriptions. The exact geometry is never directly implemented, as will be shown in the following sections. The difference between the various geometrical models vanishes as a consequence.

MULTIGRID METHODOLOGY AND IMPLEMENTATION

The basic flow equations that are solved are the Stokes equation describing a viscous flow of an incompressible, Newtonian flow and the continuity equation:

$$\underline{\nabla} p - \mu \underline{\nabla}^2 \cdot \underline{u} = 0 \quad (1)$$

$$\nabla \cdot \underline{u} = 0 \quad (2)$$

with p the pressure, μ the dynamic viscosity, u the fluid velocity, ∇ and ∇^2 denote the gradient and Laplace operators respectively. This set of equations is solved iteratively employing a finite difference technique. An initial solution is guessed. The resulting error – or residual – compared to the, yet unknown, exact solution is used to estimate a correction for the initial solution. This procedure is repeated until the numerical solution satisfies (1) and (2) within the desired limits of accuracy. Finite difference methods perform best if a regular grid of cells is employed. However, the geometry can only be described sufficiently accurate if the resolution of the grid is high. Inherently, this implies a slow converges, as errors with a relative high wavelength compared to the typical cell edge length are damped slowly in finite difference schemes [4]: the error becomes smooth, as graphically represented by Fig. 2, which implies a low convergence rate. This leads to contradicting demands on the grid resolution: a coarse grid will translates into a fast reduction of the residual, whereas only a fine grid will result in an accurate solution.

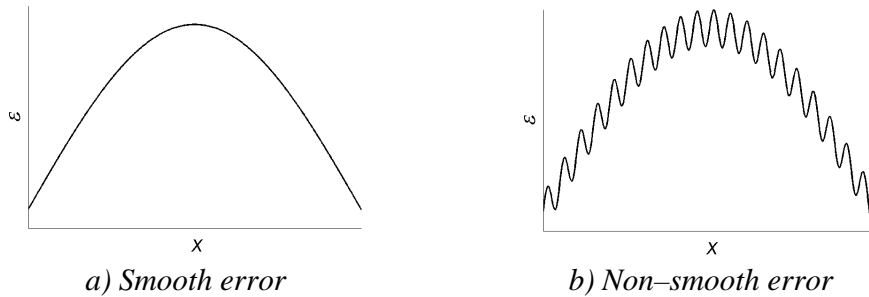


Fig. 2 Smoothness of the residual.

One of the solutions to overcome this problem is to solve the equations on different grid resolutions: the ‘Multigrid’ method. A Multigrid routine consists of three steps:

1. Relaxation: iterations performed on each grid. The number of iterations is limited, as the only objective is to obtain a smooth error. Once this is reached, the convergence rate will drop and the overall efficiency of the solver as well.
2. Restriction: transfer of the solution to a coarser grid level.
3. Prolongation: transfer of the solution to a finer grid.

A linear interpolation is employed for the restriction and prolongation. The number and order of restriction and prolongation steps depend on the type of Multigrid cycle that is followed. Here a Full MultiGrid scheme (FMG) [4] is implemented (see Fig. 3). The routine starts with an initial velocity and pressure field at the coarsest level. The velocities and pressures are transferred to a finer grid after a number of pre-relaxation. The correction for the solution on the finer grid is improved on the coarser grid levels to damp the high and low frequency errors in the estimation efficiently (circles without dot in Fig. 3), after which the velocities and pressures are corrected and a number of post-relaxations is applied (circles with dot). This cycle is repeated until the desired accuracy is obtained.

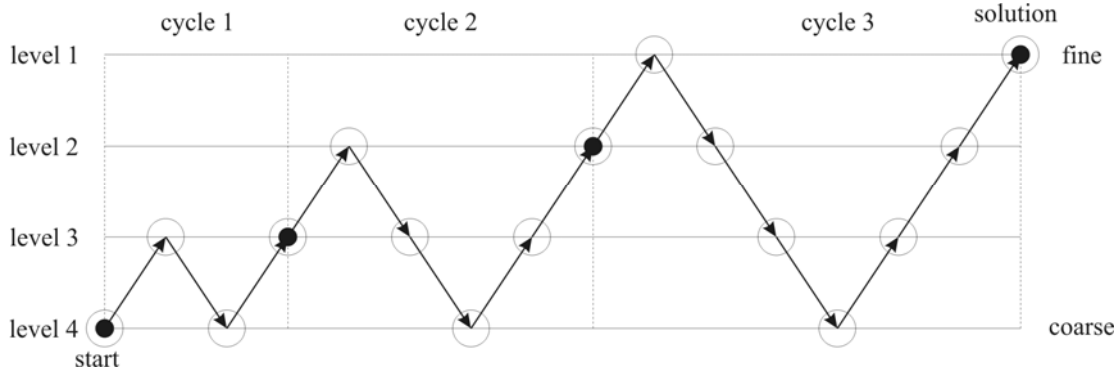


Fig. 3 A four level, three cycle full MultiGrid routine. The solution is relaxed at the circles with dots, whereas the correction is improved, using restriction and prolongation, on the circles without dots.

A staggered grid is employed: the pressures are evaluated in the cell centres, whereas the velocities are evaluated at the cell edges or faces (2D and 3D respectively), see Fig. 4. The staggered grid is required to obtain a stable solution. It can be shown rather straightforwardly that mutually independent systems of equations will be formed if a non-staggered is employed. The flow equations are discretised employing a backward and central differential scheme.

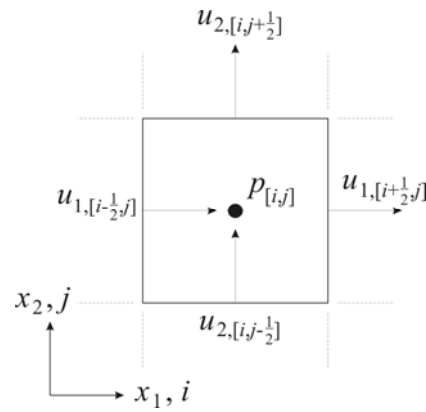


Fig. 4 A 2D staggered grid. The pressure is evaluated at the cell center, the velocities at the cell faces.

Various types of boundaries are recognized:

1. The domain boundaries where the pressures are prescribed (inlet and outlet).
2. The domain boundaries where the velocities are prescribed
3. The fibre bundle contour at which the velocities are prescribed (here set to zero, see also [3]).

An interpolation of the prescribed velocities or pressures at the boundaries is required if the degree of freedom is not defined at the boundary (for example u_1 at $x_2 = 0$, see Fig. 4). A quadratic interpolation is employed to this end.

The relaxation itself is based on a standard iterative method, in which the new estimate of a solution is based on the residual of current solution. However, a distinction must be made between the relaxation of the Stokes equation (1) and the continuity equation (2). The residual of the momentum equation in the x_1 direction r_{M_1} of the Stokes equation of the n^{th} iteration, at the face $[i-1/2,j]$ (see Fig. 4), reads:

$$r_{M_1, [i-\frac{1}{2}, j]}^{(n)} = \frac{p_{[i, j]}^{(n)} - p_{[i-1, j]}^{(n)}}{h} - \mu \frac{u_{1, [i-\frac{3}{2}, j]}^{(n)} + u_{1, [i-\frac{1}{2}, j-1]}^{(n)} - 4u_{1, [i-\frac{1}{2}, j]}^{(n)} + u_{1, [i+\frac{1}{2}, j]}^{(n)} + u_{1, [i-\frac{1}{2}, j+1]}^{(n)}}{h^2} \quad (3)$$

where p are the pressures, u_l the velocities and h the grid edge length. Note that here $h_1 = h_2 = h$, since the grid is square. The new estimate $u_{1, [i-\frac{1}{2}, j]}^{(n+1)}$ is found by adding a correction $u_{1, [i-\frac{1}{2}, j]}^{C, (n)}$ such

that the residual vanishes:

$$u_{1, [i-\frac{1}{2}, j]}^{(n+1)} = u_{1, [i-\frac{1}{2}, j]}^{(n)} + u_{1, [i-\frac{1}{2}, j]}^{C, (n)} \rightarrow u_{1, [i-\frac{1}{2}, j]}^{C, (n)} = -\frac{h^2}{4\mu} r_{M_1, [i-\frac{1}{2}, j]}^{(n)} \quad (4)$$

The new estimate for the velocity in the x_2 direction is obtained in the same way. A slightly different correction is found for the cells at the domain and fibre bundle boundaries.

The relaxation of the continuity equation is performed over a cell rather than on a single cell edge. A distributive relaxation is applied for the continuity equation. This implies that a single correction for the velocities at the cell edges of cell $[i, j]$ is applied, whereas the pressure in the cell $[i, j]$ as well the pressures in the neighbouring cells are corrected, as shown in Fig. 5.

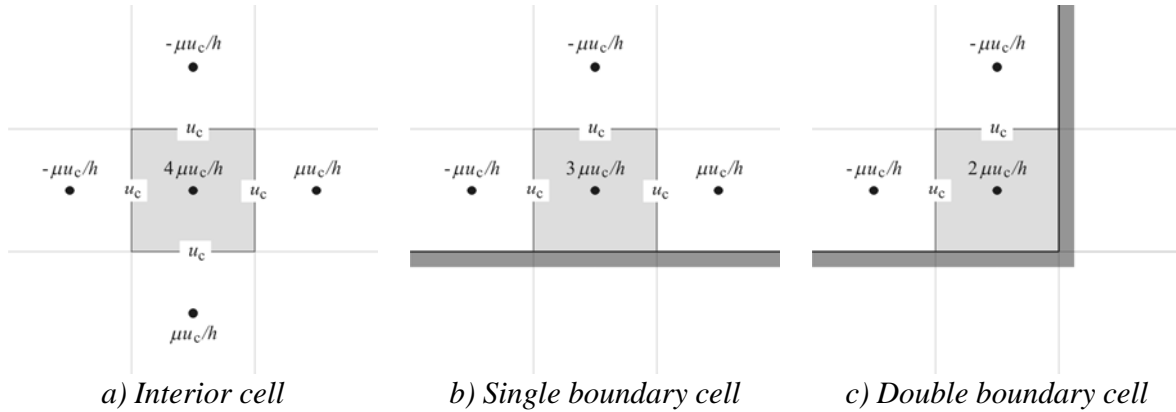


Fig. 5 Distributive relaxation: velocities at the cell edges are corrected with a single correction, where as the pressures in the central cell and in its neighbouring cells are corrected simultaneously.

The residual of the continuity equation (2) r_C is employed to determine the correction on the velocities $u_{[i, j]}^{C, (n)}$:

$$r_{C, [i, j]}^{(n)} = \frac{u_{1, [i-\frac{1}{2}, j]}^{(n)} - u_{1, [i+\frac{1}{2}, j]}^{(n)}}{h_1} + \frac{u_{2, [i, j-\frac{1}{2}]}^{(n)} - u_{2, [i, j+\frac{1}{2}]}^{(n)}}{h_1} \quad (5)$$

Applying the corrections as indicated in Fig. 6 and demanding the residual to vanish after the correction is applied leads to the following expression for the correction:

$$u_{[i,j]}^{C(n)} = \frac{h}{4} r_{C,[i,j]}^{(n)}, \text{ with: } \begin{aligned} u_{1,[i-\frac{1}{2},j]}^{(n+1)} &= u_{1,[i-\frac{1}{2},j]}^{(n)} - \frac{h}{4} r_{C,[i,j]}^{(n)} & u_{1,[i+\frac{1}{2},j]}^{(n+1)} &= u_{1,[i+\frac{1}{2},j]}^{(n)} + \frac{h}{4} r_{C,[i,j]}^{(n)} \\ u_{2,[i,j-\frac{1}{2}]}^{(n+1)} &= u_{2,[i,j-\frac{1}{2}]}^{(n)} - \frac{h}{4} r_{C,[i,j]}^{(n)} & u_{2,[i,j+\frac{1}{2}]}^{(n+1)} &= u_{2,[i,j+\frac{1}{2}]}^{(n)} + \frac{h}{4} r_{C,[i,j]}^{(n)} \end{aligned} \quad (6)$$

This second correction changes the residuals in Stokes equation, which is compensated by corrections on the pressures ($p_{[i,j]}^{C(n)}$, $p_{[i\pm 1,j]}^{C(n)}$ and $p_{[i,j\pm 1]}^{C(n)}$). In other words, the equations

$$r_{M_1,[i\pm 1,j]}^{(n)} = 0; \quad r_{M_2,[i,j\pm 1]}^{(n)} = 0 \quad (7)$$

remain valid after the corrections are applied. The distributive relaxation differs at the cells near an internal or external boundary as shown in Fig. 5b and c. Note that the boundary can either be internal or external.

RESULTS AND DISCUSSION

The performance of a Multigrid solver in a two-dimensional domain including an impermeable, circular shaped obstruction (representing a fibre bundle) as shown in Fig. 6 is tested. The fibre bundle is assumed to be part of a regular, square packed array of fibre bundles. Hence, symmetric boundary conditions are applied for the velocities on the edges perpendicular to the pressure gradient, as shown in Fig. 7.

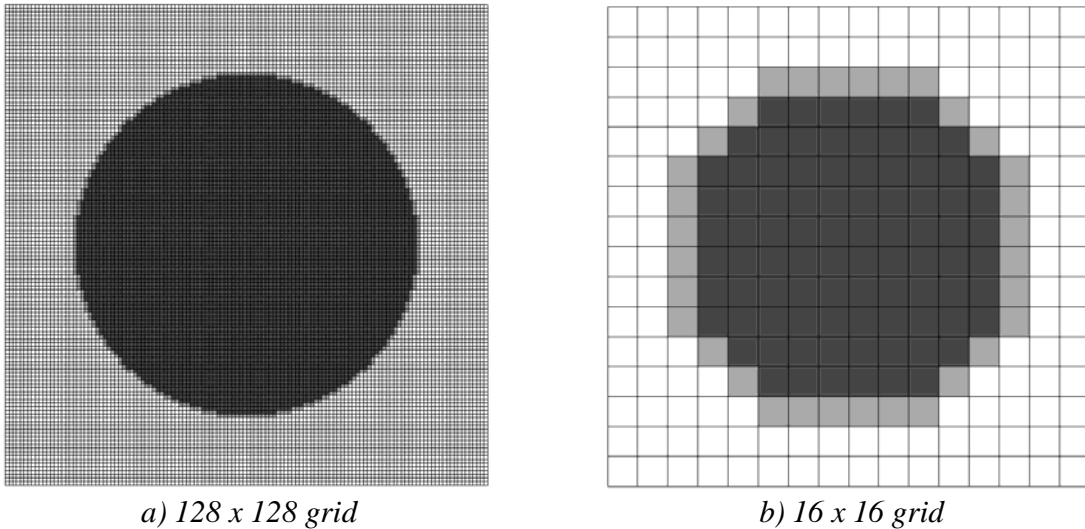


Fig. 6 Coarse and fine grid representation of a circular bundle cross-section in a two-dimensional domain. The black area refers to cell in the interior of the bundle, the gray to the cells on the edge of the bundle and the white to the fluid domain.

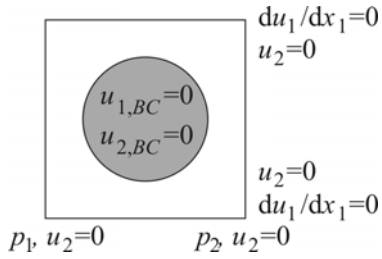


Fig. 7 Boundary conditions applied for a cell in a regular, square packed array of impermeable fibre bundles.

The results are compared to results of similar exercises found in the literature. The solution is also compared to experimental data and a CFX solution. The settings of the Multigrid solver are presented in Table 1 and the properties of the fluid and domain, and the applied pressure gradient are presented in Table 2.

Table 1 Iteration settings for the Multigrid solver as applied here

	Iteration sweeps [#]
Pre-relaxations	10
Post-relaxations	10
Restriction	10
Interpolation	10
Coarse grid	30
Number of cycles	4

Table 2 Fluid and domain properties; applied pressure gradient

Variable		unit
∇p_x	-50	[Pa·m ⁻¹]
μ	$33 \cdot 10^{-3}$	[Pa·s]
L	0.1	[m]
n	512×512	[-]
V_f	0.1 - 0.725	[-]

The resulting velocity and pressure distributions are shown in Fig. 8. The pressure gradient is applied in the x_1 direction, which is the vertical direction in the graphs. The fibre bundle boundary is indicated in the first image, but also clearly recognizable in the other images.

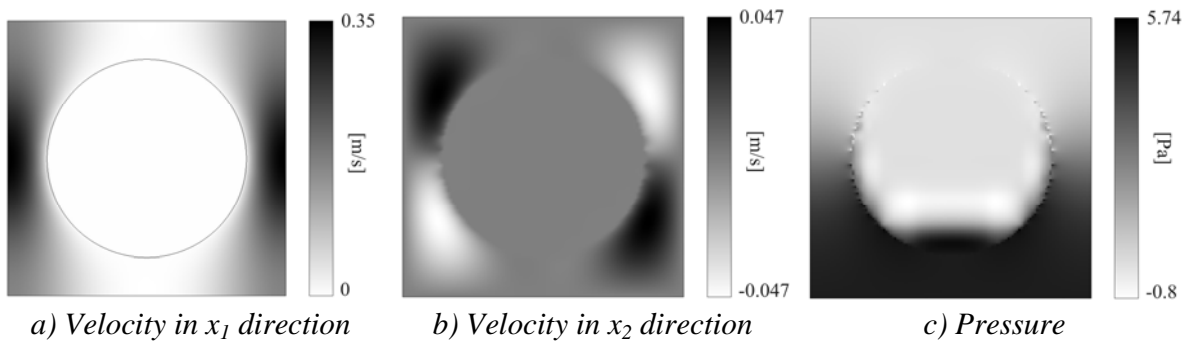


Fig. 8 Velocity and pressure calculated by the Multigrid program.

The error norm of the residual and the required computation time on a single CPU (2.0GHz, 1Gb RAM) for three FMG simulations and three standard, single grid finite difference simulations ('single grid') are presented in Table 3. The Multigrid routine provides a significant improvement in terms of computational effort, while the accuracy is still well within acceptable limits. Note, that this implies that the inaccurate approximation of the fibre bundle geometry at the coarser grid

resolutions (Fig. 6b versus 6a) hardly affects the final solution. Apparently, the error introduced at the coarser levels is efficiently reduced by the finer grid levels.

Table 3 Performance of the Full MultiGrid routine for various grid sizes compared to the equivalent standard finite difference ('single grid') solution in terms of computation time and error norm of the residual. A fibre content of 0.4 was used. The coarsest grid resolution is given between brackets.

grid		levels	Full MultiGrid		Single grid	
			time [s]	ϵ [-]	time [s]	ϵ [-]
32 × 32	(8 × 8)	3	4.44	4.31×10^{-4}	45.15	1.31×10^{-9}
128 × 128	(8 × 8)	5	86.72	3.96×10^{-5}	631.28*	3.85×10^{-4}
512 × 512	(32 × 32)	5	1362.70	6.40×10^{-3}	>80000**	7.50×10^{-4}

* maximum number of iteration of 1000 reached

** stopped manually after 22 hrs and 8000 iterations

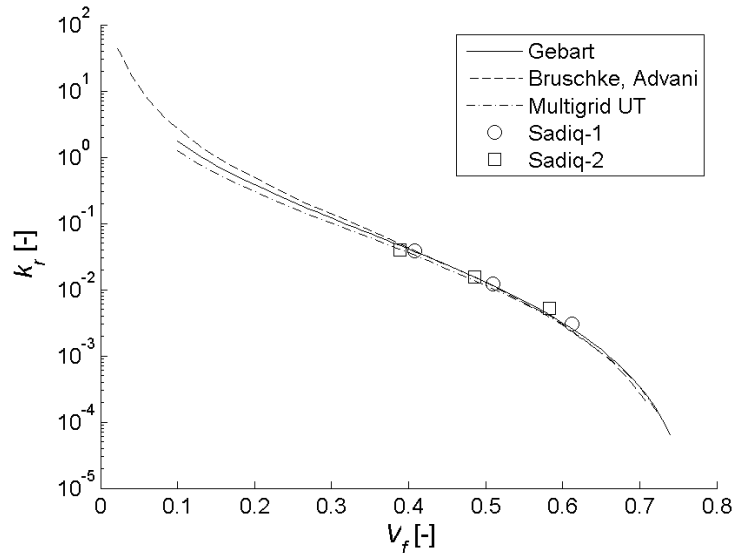


Fig. 9 Comparison of the dimensionless permeability calculated by the Multigrid solver and numerical and experimental results found in the literature.

The velocity field obtained and the pressure gradient applied are used to calculate the permeability of the flow domain. The calculated values for a wide range of fibre contents are compared to the numerical results obtained by Gebart [5] and Bruschke and Advani [6] and the experimental results of Sadiq [7]. Fig. 9 shows that the permeabilities calculated by the Multigrid solver correspond to the results previously obtained.

CONCLUSIONS

A Multigrid solver was implemented to predict the flow through a fibre reinforcement and hence the permeability. As a first step, the solver is developed to solve the flow around circular obstruction in a square domain. The strength of the Multigrid algorithm is its high convergence

rate compared to standard finite difference schemes. However, the price of this efficiency can be an inadequate representation of the internal geometry of the textile reinforcement at the coarsest grid points. This is shown to be of little influence on the stability of the solution. Note that this implies that the exact description of the internal geometry may not be as important as would be expected.

It is proven that the accuracy and CPU-calculation time are sufficiently good to continue the development of more complex structures and the incorporation of lower level flow phenomena. Research has started [3], in parallel to the development of the solver, to investigate the role of the micro level flow and the implementation of boundary conditions for the Multigrid solver, which is the next step forward.

ACKNOWLEDGEMENTS

The authors would like to thank Reden B.V. and Ten Cate Advanced Composites for their support, as well as the University of Twente on the theory behind the Multigrid methodology.

REFERENCES

1. S.V. Lomov, T. Truong Chi, I. Verpoest, T. Peeters, D. Roose, P. Boisse, A. Gasser, "Mathematical Modelling of Internal Geometry and Deformability of Woven Preforms", *International Journal of Forming Processes*, 6:413-442, 2003.
2. F. Robitaille, A.C. Long, C.D. Rudd, "Geometrical Modelling of Textiles for Prediction of Composite Processing and Performance Characteristics", *Plastics, Rubber and Composites*, 31(2):66-75, 2002.
3. W.J.B. Grouve, R. Akkerman, "An Idealised BC for Meso-Scale Analysis of Textile Impregnation Processes", Proceedings of FPCM-9, Montréal, Canada, 2008.
4. C.H. Venner and A.A. Lubrecht, "Multilevel Methods in Lubrication", Tribology Series 37, Elsevier, Amsterdam, 2000.
5. R.B. Gebart, "Permeability of Unidirectional Reinforcements for RTM", *Journal of Composite Materials*, 26(8):1100-1133, 1992.
6. M.V. Brusckhe, S.G. Advani, "Flow of Generalised Newtonian Fluids across a Periodic Array of Cylinders", *Journal of Rheology*, 37(3):479-496, 1993.
7. T.A.K. Sadiq, S.G. Advani, R.S. Parnas, "Experimental Investigation of Transverse Flow Through Aligned Cylinders", *International Journal of Multiphase Flow*, 21(5):755-774.